On the driving factors of the future changes in the wintertime Northern-Hemisphere atmospheric waviness

A. Yamamoto[1] and P. Martineau[2]

[1]J. F. Oberlin University, Machida, Tokyo, Japan
[2]Japan Agency for Marine-Earth Science and Technology, Yokohama, Kanagawa, Japan

Key Points:

- Historical simulations exhibit biases in Northern Hemisphere wintertime climatological waviness, mostly ameliorated with higher resolution
- High-resolution models mitigate general reduction seen in projected Northern Hemisphere wintertime waviness in future simulations
- Sensible heat fluxes play a crucial role in both historical biases and future reductions in waviness, highlighting the key role of the ocean

Corresponding author: Ayako Yamamoto, `yamamoto_a@obirin.ac.jp`

Abstract
The link between atmospheric waviness and extreme weather events carries significant socioeconomic implications. However, future atmospheric waviness trends remain elusive due to uncertainties arising from diverse definitions and insufficient dynamical formalism in existing metrics. This study employs a local wave activity (LWA) metric, whose prognostic equation links wave activity changes to forcing mechanisms, to assess wintertime Northern Hemisphere waviness in ERA5 and HighResMIP datasets. The models generally exhibit high fidelity in reproducing observed waviness, particularly improving with higher resolutions. The LWA, generated by low-level meridional heat flux, reveals biases in the historical period stemming from underestimation of the source. Future projections exhibit reduction in LWA, primarily due to suppressed LWA generation, which is mitigated by higher resolution models. We found that both biases and reduction of the LWA source are closely associated with sensible heat fluxes from the ocean to the atmosphere, highlighting the potential impacts of resolving ocean currents.

1 Introduction

In the mid-latitude atmosphere, surface weather is tightly coupled with fluctuations of the circulation aloft that is associated with the propagation of atmospheric waves. These atmospheric waves in turn are closely linked to the frequency and severity of extreme weather events. As such, there has been a growing interest in the past decade to characterize and understand changes in waviness of the midlatitude circulation.

Based on a metric quantifying the meandering of an arbitrary geopotential height contour, Francis and Vavrus (2012) claimed that the waviness of the extratropical Northern Hemisphere (NH) circulation had been amplifying as a consequence of the enhanced near-surface warming over the Arctic, a phenomenon known as Arctic amplification. This claim, however, has been disputed by Barnes (2013), who argued that the positive trend found in their study likely stems from an artefact of the metric used. Using an improved metric that is also based on geopotential height, she has highlighted a lack of robust trends in waviness in the historical record. Since then, many studies have assessed waviness trends using various methods based on the meridional excursion of contours of different variables such as potential vorticity (PV) (Röthlisberger et al., 2016) and geopotential height (Cattiaux et al., 2016; Di Capua & Coumou, 2016; Martin, 2021), or the amplitude of circulation anomalies with respect to the zonal mean (Coumou et al., 2015). It is, however, generally challenging to draw an unanimous conclusion on the observed and future trends of waviness from these diverse metrics.

Notably, Screen and Simmonds (2013) emphasized that assessments of trends in waviness are sensitive to whether waves are considered as meandering of contours, or zonal anomalies. Chen et al. (2015) and Martineau et al. (2017) attempted to reconcile these two concepts by using a metric that takes into account both the meridional displacements of geopotential height contours and the amplitude of the enclosed anomalies. These new metrics, together with the predecessors, however, suffer from not being grounded in a dynamical formalism. As such, no prognostic equation links changes in these waviness metrics to forcing mechanisms.

A waviness metric called local wave activity (LWA) developed by Huang and Nakamura (2016) overcomes this drawback, thereby possibly leading to acquiring a better understanding in the changes in waviness. LWA is a conservative quantity for quasigeostrophic flows, whose governing equation links LWA time tendencies to dynamical processes. Generalizing the linear, small-amplitude theory to eddies of arbitrary amplitude, LWA has demonstrated its usefulness in capturing extreme jet meandering events such as atmospheric blocking, while enabling the diagnosis of the physical processes that drive waviness (Huang & Nakamura, 2016; Nakamura & Huang, 2018).

Here, we employ the LWA budget analysis to assess historical and future waviness. In view of a growing body of evidence that enhanced model resolution improves the representation of transient eddies (Boville, 1991) and large-scale atmospheric variability (Davini & D'Andrea, 2020; Athanasiadis et al., 2022), here we apply LWA metric to a suite of low- and high-resolution climate models and a reanalysis dataset. Our study aims to 1) evaluate the fidelity of state-of-the-art climate models in reproducing the waviness in the current climate, 2) diagnose changes in the atmospheric waviness in the future climate, and 3) investigate the benefits of using high-resolution models.

2 Dataset Used

We utilize selected model output from the High Resolution Model Intercomparison Project (HighResMIP; Haarsma et al., 2016). HighResMIP is a coordinated effort to systematically assess robust advantages of increasing horizontal resolution in models, given that simulation of a multitude of atmospheric and oceanic phenomena have been reported to improve with higher horizontal model resolution (see reviews in Haarsma et al., 2016). Here, "high-resolution" denotes a resolution higher than 50 km or 0.25° for the atmosphere and the ocean respectively.

We use coupled model runs from five sets of HighResMIP models (Table S1), each of which meets the following criteria: A model 1) has both low- and high-resolution versions, 2) has daily three-dimensional zonal and meridional wind speed and temperature, and 3) has all the meteorological fields extrapolated under the topography. The latter two criteria are necessitated for the LWA computation. Table S1 illustrates that the range of high and low resolutions depends entirely on the model being used. Here, regardless of the actual model resolution, we categorize lower and higher resolution of each model set as "low-resolution" and "high-resolution" models. All three-dimensional fields are provided on the common eight pressure levels (1000, 850, 700, 500, 250, 100, 50, and 10 hPa). In addition to the aforementioned three-dimensional variables, we use monthly sensible heat flux data. Here, we analyze boreal winter (December-January-February; DJF) seasons for years 1960-1995 from historical runs, and years 2015-2050 from the future runs. Since ECMWF-IFS models only provide historical runs, they are only used for the assessment of model fidelity and the historical LWA budget analysis. We use one ensemble member from each model, and each dataset is interpolated onto 2°× 2° horizontal grid prior to analyses.

Additionally, the fifth generation ECMWF atmospheric reanalysis dataset (ERA5; Hersbach et al., 2020) is used as a reference atmospheric state for the historical period. ERA5 data are also interpolated on the same common grid and temporal resolution as HighResMIP prior to the analyses.

3 Local Wave Activity (LWA) diagnosis

In this study, we use local wave activity (LWA; Huang & Nakamura, 2016) as a measure of waviness. LWA is a generalization of the finite amplitude wave activity that quantifies wave activity in the pressure-latitude plane (Nakamura & Solomon, 2010) to its three-dimensional representation. The LWA quantifies waviness based on the meridional displacements of the quasi-geostrophic potential vorticity (QGPV) substance. It is advantageous over classical definitions of eddies by its ability to quantify and provide a conservation relation that holds for eddies of finite (as opposed to small) amplitude.

LWA (A) quantified at each longitude (λ), latitude (ϕ), height (z), and time (t) is defined as follows:

$$A(\lambda, \phi, z, t) = -\frac{a}{cos\phi} \int_0^{\Delta\phi} q_e(\lambda, \phi, \phi', z, t) cos(\phi + \phi') d\phi' \tag{1}$$

where a is the planetary radius, and q_e is a QGPV anomaly with respect to its zonally symmetric reference state, $q_{ref}(\phi, z, t)$, defined as

$$q_e(\lambda, \phi, \phi', z, t) = q(\lambda, \phi + \phi', z, t) - q_{ref}(\phi, z, t). \tag{2}$$

q_{ref} is computed by zonalizing the QGPV contours while preserving the enclosed areas (Nakamura & Solomon, 2010). In this formulation LWA is by definition a positive definite quantity, regardless of whether it is assessed over sectors where the zonal flow is perturbed by troughs or ridges (Huang & Nakamura, 2016).

When averaged over a season, LWA contains both stationary and transient eddy components, whose straightforward partitioning is hindered partly by the fact that a reference state (Equation 2) is based on the Lagrangian average of QGPV. Here, following Huang and Nakamura (2017), we estimate the stationary component by computing LWA from the temporal mean of QGPV, and the transient component as a difference between the total LWA and the stationary component.

The time tendency of LWA is defined as follows:

$$\frac{\partial}{\partial t}\langle A\rangle cos\phi = \underbrace{-\frac{1}{acos\phi}\frac{\partial\langle F_\lambda\rangle}{\partial\lambda}}_{(i)} + \underbrace{\frac{1}{acos\phi}\frac{\partial}{\partial\phi}\langle u_e v_e cos^2(\phi)\rangle}_{(ii)} + \underbrace{\frac{fcos\phi}{H}\left(\frac{v_e\theta_e}{\partial\tilde{\theta}/\partial z}\right)_{z=0}}_{(iii)} + \underbrace{\langle\dot{A}\rangle cos\phi}_{(iv)}, \tag{3}$$

where $\langle\cdots\rangle$ denotes the density-weighted vertical average. The terms (i) and (ii) represent zonal and meridional LWA flux convergence, respectively, whereas the term (iii) represents low-level eddy meridional heat flux, which describes vertical LWA flux at the lower boundary. The term (iv) denotes residual, which results from non-quasigeostrophic processes, including diabatic processes such as vertical transport of low PV air from the lower troposphere fuelled by latent heat release (Grams & Archambault, 2016; Pfahl et al., 2015; Yamamoto et al., 2021; Neal et al., 2022).

The zonal LWA flux $\langle F_\lambda\rangle$ in term (i) is composed of three terms:

$$\langle F_\lambda\rangle = \underbrace{\langle u_{ref}Acos\phi\rangle}_{(a)} + \underbrace{a\left\langle\int_0^{\Delta\phi} u_e q_e cos(\phi+\phi')d\phi'\right\rangle}_{(b)} + \underbrace{\frac{cos\phi}{2}\left\langle v_e^2 - u_e^2 - \frac{R}{H}\frac{e^{-\frac{\kappa z}{H}}}{\partial\tilde{\theta}/\partial z}\theta_e^2\right\rangle}_{(c)} \tag{4}$$

The terms (a) and (b) of Equation 4 make up of advective flux of LWA. Here, we investigate these density-weighted vertical averages, given the quasi-barotropic nature of these phenomena.

4 LWA Biases in Historical Runs

Comparison of the climatological wintertime LWA spatial distribution in the historical period for ERA5 and multi-model mean (MMM) of all the climate models used (top two panels of Figure 1a) reveals that the general features in the reanalysis are well captured by the MMM, including the two distinct maxima observed over the Pacific and Atlantic sectors. This spatial distribution resembles that of wintertime climatological blocking frequency, a weather event that disturbs the path of the jet stream and consequently affects waviness (see Figure 2 of Woollings et al., 2018).

The MMM bias of LWA against ERA5 in the historical record (Figure 1a lower-left panel) illustrates that waviness maximum found over Europe is underestimated by the models by approximately 10%, which is also fairly analogous to the well-known common model bias for the European blocking frequencies. This model bias in blocking stems from a lack of anticyclonic wave breaking and bias in the eddy-driven jet, which, while alleviated compared to its predecessors, are still prevalent in CMIP6 models (Davini & D'Andrea, 2020; Athanasiadis et al., 2022). Thus, the negative bias found in the simulated LWA also likely reflects these biases in models. Decomposition of the observed and MMM LWA into its stationary and transient components (Figure S1) reveals that this negative bias stems solely from the stationary component, hinting that underestimation in blocking frequency has an imprint on the suppressed time-mean ridge. Conversely, the MMM LWA over much of the mid-latitude Pacific and also over Eurasia overestimates the observed strength of waviness. While the excessive LWA over the Pacific stems from both stationary and transient components, it is mostly due to transient component over Eurasia (Figure S1). The sectors where the MMM LWA positive biases are found correspond to where the depth-averaged MMM zonal wind exhibits negative biases against ERA5, suggesting that a wavier flow is accompanied by a reduction in zonal winds (Figure S2). Inconsistencies from this relationship possibly arise due to the surface forcing over the land, and from averaging multiple realizations of the atmosphere and time. The lower-right panel of Figure 1a illustrates the difference in model bias between high-resolution models and low-resolution counterparts. It is shown that biases in the high-resolution models are generally reduced over eastern Eurasia and southwestern edge of Europe, though slightly amplified over the northeastern Europe.

A Taylor diagram (Figure 1b) illustrates the reproducibility of the LWA spatial pattern in the historical record by each model. It is evident that each model simulates the climatological LWA pattern fairly well, which typically improves with high-resolution models (up-pointing triangles) compared to their low-resolution counterparts (down-pointing triangles), while the extent of improvement highly depends on the model. HiRAM-SIT-HR is an exception, which, despite having a high correlation, displays much lower standard deviation compared to HiRAM-SIT-LR. As shown in Figure S3, HiRAM-SIT-HR shows a weaker climatological LWA compared to ERA5, particularly over the North Atlantic sector. As whether including this model or not did not qualitatively change the results for the rest of the analyses, we retain this model in the rest of our analyses.

5 LWA budget analyses in the historical period

To show how the LWA budget is upheld, Figure 2 illustrates the climatology of the first three forcing terms on the right-hand side of Equation 3. It is evident that for both ERA5 and the MMM low-level meridional flux (Figure 2c) acts as a source of LWA over the storm track regions of both the Atlantic and Pacific sectors (encircled by black contours) as well as over the Gulf of Alaska, consistent with Huang and Nakamura (2017). While the two maxima of low-level meridional flux over the Pacific are locally confined, the region of positive (i.e., poleward) low-level meridional heat flux over the Atlantic sector spans further to the northeast following the North Atlantic Current, an extension of the warm Gulf Stream. Huang and Nakamura (2017) attributed a significant portion of this elongated signal over the Atlantic to the quasi-stationary zonal asymmetry in low-level potential temperature which arises from the underlying sea surface temperature (SST) distribution and the accompanying meridional wind. This positive low-level meridional heat flux is largely compensated by the zonal advective flux divergence, such that LWA is redistributed mainly downstream (Figure 2a). The eddy momentum flux divergence (Figure 2b) also acts as a sink though to a much lesser extent.

When compared to ERA5, models tend to underestimate the low-level meridional heat flux upstream of LWA maximum found over the Atlantic sector (Figure 2 third column). This underestimation of the LWA source appears to stem from the suppressed surface sensible heat flux (SHF) from the ocean to the atmosphere in the vicinity of so-called Northwest Corner, the beginning of the North Atlantic Current (Figure S4). This region coincides with where a strong cold SST bias is commonly found in the ocean-sea-ice simulations (Tsujino et al., 2020), which gives rise to the negative SHF bias. Together with the overestimation of SHF over the North Atlantic south of Iceland, these SHF biases lead to the subdued meridional heat flux, which results in suppressed LWA source over this region. Consequently, the downstream redistribution of LWA by zonal advective flux divergence is weaker than ERA5 (i.e., positive bias), resulting in the underestimation of LWA over the Atlantic sector. This result is consistent with Athanasiadis et al. (2022), who showed that the reduced cold SST bias at the Northwest Corner generally leads to improved representation of European blocking in climate models, due to ameliorated low-level baroclinicity. On the contrary, overestimation of simulated LWA over much of the rest of the NH midlatitudes stems from excessive LWA production by low-level meridional heat flux found over the eastern edge of Eurasian continent and the vicinity of Gulf of Alaska (Figure 2c), which results in extra LWA advection downstream over both of these regions (Figure 2a). The excessive LWA sources are likely attributable to positive SHF bias over Japan Sea and off the west coast of North America (Figure S4). In both cases, the role of eddy momentum flux divergence (Figure 2b) is comparatively negligible. The last column of Figure 2 illustrates that higher resolution models systematically reduce the suppressed low-level meridional heat flux bias over the western edge of the Atlantic LWA maximum, leading to the improved model fidelity in LWA. This better model fidelity should also be ascribable to the ameliorated SHF (Figure S4).

6 Historical vs. future LWA

The future LWA projection features a general reduction in LWA, particularly at the southern flanks of both maxima over the Atlantic and Pacific sectors and over the west coast of North America (Figure 3a third column), which are all mostly attributable to the stationary component (Figure S5). Reduction over the northern flanks of LWA maxima over the Atlantic is mitigated with high-resolution models compared to the low-resolution counterparts (Figure 3a fourth column), which is also solely due to the stationary component (Figure S5). An exception for this general reduction in waviness is found near Barents-Kara Sea, where over three quarters of models investigated suggest projected increase in waviness. This region coincides with where a statistically significant increase in LWA linear trend is found in the historical period (Nakamura & Huang, 2018, see their Figure S6).

The LWA budget retains its balance in the future projection, such that the low-level meridional heat flux acts as the primary LWA source (Figure 3d), while zonal advective flux divergence (Figure 3b) acts as the primary sink over both the Atlantic and Pacific sectors, redistributing LWA downstream. The low-level meridional heat flux particularly in the north of Iceland and Japan is projected to decrease in the future, which results in reduced downstream redistribution of LWA by zonal advective flux divergence (i.e., increase in convergence) and reduction in LWA. We found that these areas coincide with reduced transfer of SHF from the ocean to the atmosphere in the extratropics, while closer to the pole, increased SHF is released to the atmosphere, due likely to sea ice melting in the future (Figure S6). These contrasting SHF change in turn results in the reduced meridional heat flux. Intriguingly, this future reduction in both LWA source and sink is damped in the majority of high-resolution models, resulting in less projected reduction of LWA. Figure S6 further reveals a strong positive signal over Kuroshio extension and weak but significant positive signal over the North Atlantic Current in SHF of high-resolution models, indicating that the suppression in reduction of LWA is attributable to resolving larger ocean heat fluxes released from the western boundary currents. The waviness increase found near Barents-Kara Sea, in contrast, is characterized by amplified divergence of zonal advective flux, without any increase in LWA source by low-level meridional heat flux (Figure S7), possibly indicating an enhanced waviness due to diabatic source.

Figure 4a summarizes the contribution by each term comprised in the LWA time tendency equation (Equation 3) along with the residual term obtained by assuming the tendency to become zero climatologically, over the Pacific Sector (encircled area on Figures 2 and 3). It is evident that (iii)low-level meridional heat flux stands alone as the primary LWA source over the Pacific sector. For ERA5, the LWA production is balanced by (i)zonal advective flux divergence (73.2%), (ii)eddy momentum flux divergence (16.7%), and (iv)residual (10.1%). For the low-resolution models in historical run, LWA production is overestimated by 12.4% compared to ERA5 on average, which is reduced to 3.4% with high-resolution counterparts. LWA production in the future decreases compared to the historical run by 6.9% and 6.7% for low- and high-resolution models, respectively.

Figure 4b) summarizes the balance of each term over the Atlantic Sector. In contrast to the Pacific case, it is apparent that (iv)residual acts as a secondary LWA source, along with (iii)low-level meridional heat flux. This is consistent with the fact that this Atlantic Sector coincides with the outflow region of a large-scale cross-isentropic ascent associated with extratropical cyclones called a warm conveyor belt (WCB; Madonna et al., 2014), which can increase the upper-level waviness by bringing low-PV air from the lower troposphere (Grams & Archambault, 2016; Pfahl et al., 2015; Yamamoto et al., 2021). For ERA5, (iii)low-level meridional heat flux explains 62.6% of the LWA production, whereas the rest is due to (iv)residual. 90.9% of this LWA production is redistributed by (i)zonal advective flux divergence. Underestimation of the LWA source with low- and high-resolution models compared to ERA5 amount to 11.4% and 12.9%, respectively, while excluding HiRAM-SIT models enhances agreement with ERA5 for high-resolution models (Figure S8). In the future LWA production decreases compared to the historical run, by 16.1% for low-resolution models, and by 11.9% for high-resolution models, which is primarily balanced by the decrease in (i)zonal advective flux convergence for both sets of models.

7 Conclusion and Discussion

In this study, by applying a local wave activity (LWA) metric to both a suite of low- and high-resolution climate models and a reanalysis dataset, we characterized the historical model bias and future changes in Northern Hemisphere wintertime climatological waviness, and identified causes behind them.

We found that both the biases in historical LWA source and reduction in LWA source in the future are associated with biases and reduction in sensible heat fluxes (SHF), respectively. Higher resolution better resolves SHF and suppresses both biases and reduction of LWA, thus pointing towards the importance of having higher ocean resolution for an accurate future waviness projection. In the present study we have highlighted the potential role of the ocean for the atmospheric waviness from a climatological perspective. Understanding how sensitive waviness is to oceanic variability on shorter time scales also has important implications.

Additionally, the analysis illustrated that the residual term serves as a source over the Atlantic on average, which undergoes reduction in the future. This result appears to suggest a projected reduction in fuelling low potential-vorticity air from low latitude and low altitude via warm conveyor belt (WCB) over the region (Grams & Archambault, 2016; Pfahl et al., 2015; Yamamoto et al., 2021). This assumption, however, is in apparent odds with a recent study which found a general increase in the WCB intensity in a future simulation (Joos et al., 2023). A quantitative assessment of how much low potential-vorticity air sets waviness in the changing climate remains to be investigated.

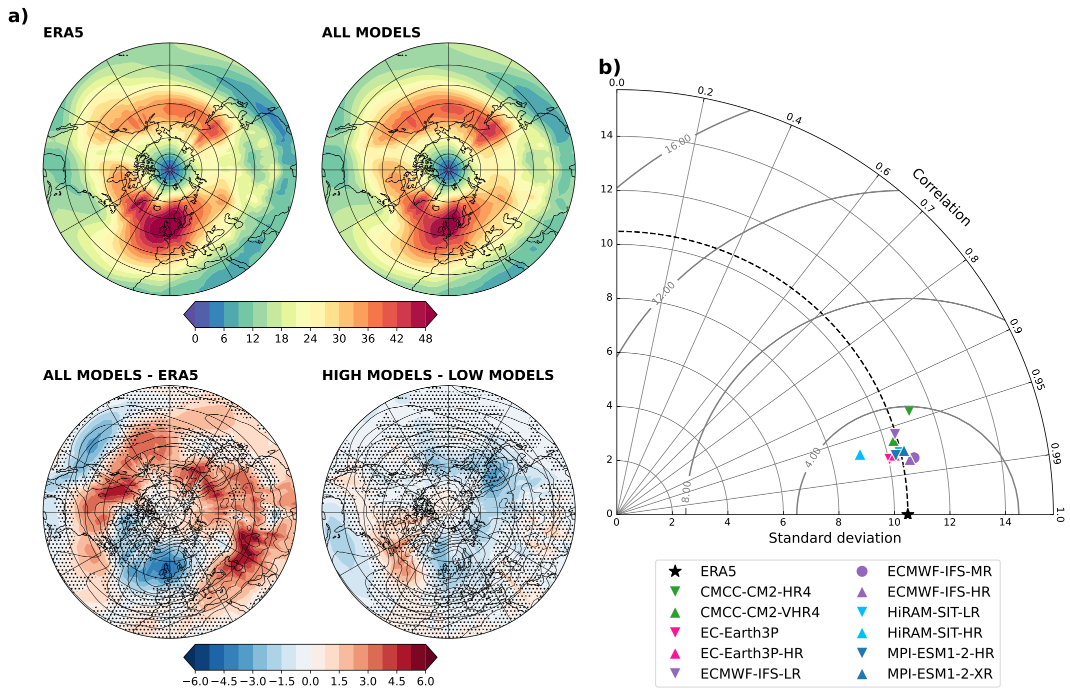

Figure 1. a) DJF LWA climatology [m s^{-1}] computed using ERA5 (top left) and all HighResMIP models (top right), LWA climatology difference between all HighResMIP models and ERA5 (bottom left) and difference between high-resolution models and low-resolution models (bottom right). Unstippled areas in the last two columns show a mean difference sign agreeing with at least three-quarters of models, and black contours indicate ERA5 LWA DJF climatology. b) Taylor diagram displaying a statistical comparison of LWA computed with HighResMIP model simulations against that computed with ERA5.

8 Availability Statement

HighResMIP and ERA5 data used in this study are available from the ESGF (`https://esgf.llnl.gov/`) and CDS (`https://cds.climate.copernicus.eu`) platforms. A python library to compute LWA was obtained from `https://github.com/csyhuang/hn2016_falwa`.

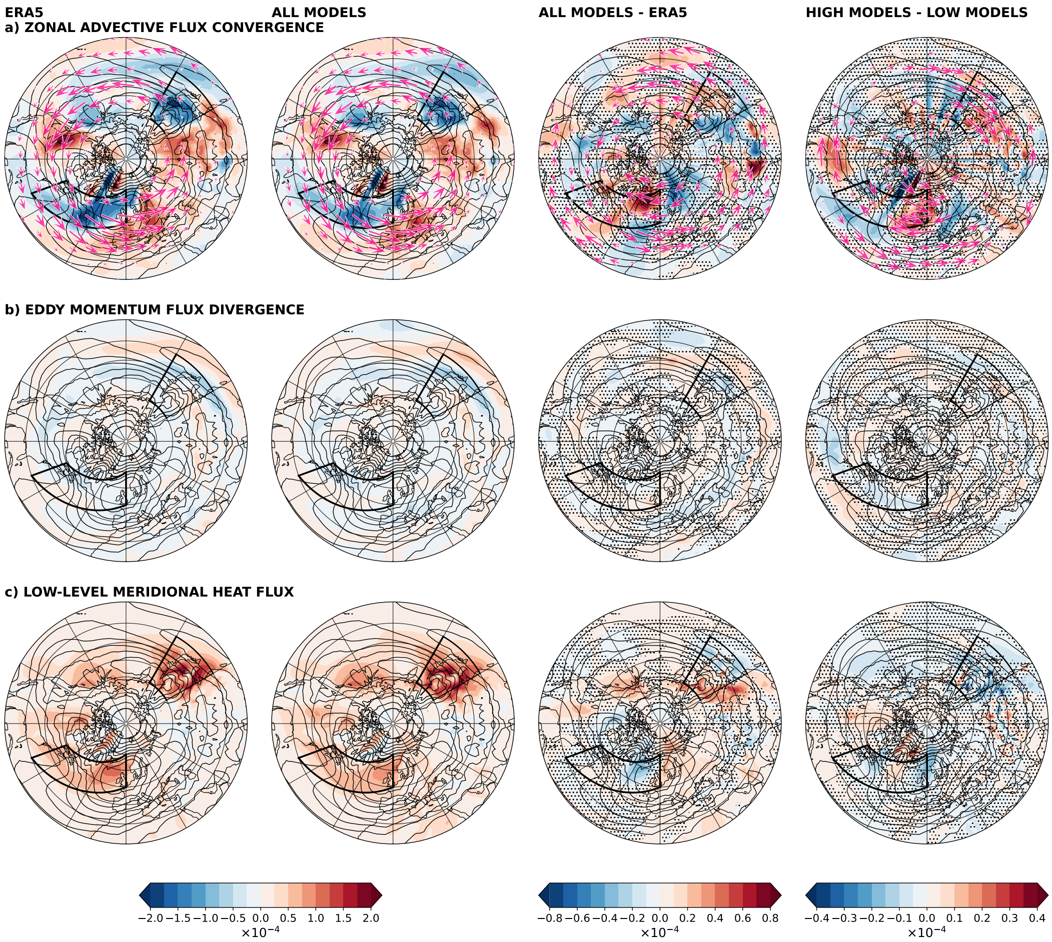

Figure 2. Historical DJF climatology of three terms comprised in the LWA time tendency equation (Equation 3): a) Zonal advective flux convergence (shade) and advective flux of LWA (arrows), b) eddy momentum flux divergence, and c) low-level meridional heat flux. Each column denotes results with ERA5 (left column), with all HighResMIP models (second column), difference between all models and ERA5 (third column), and difference between high-resolution models and low-resolution models (last column). Black contours indicate ERA5 LWA DJF climatology, and unstippled areas in the last two columns show a mean difference sign agreeing with at least three-quarters of models. Black thick lines encircle the areas investigated in Figure 4.

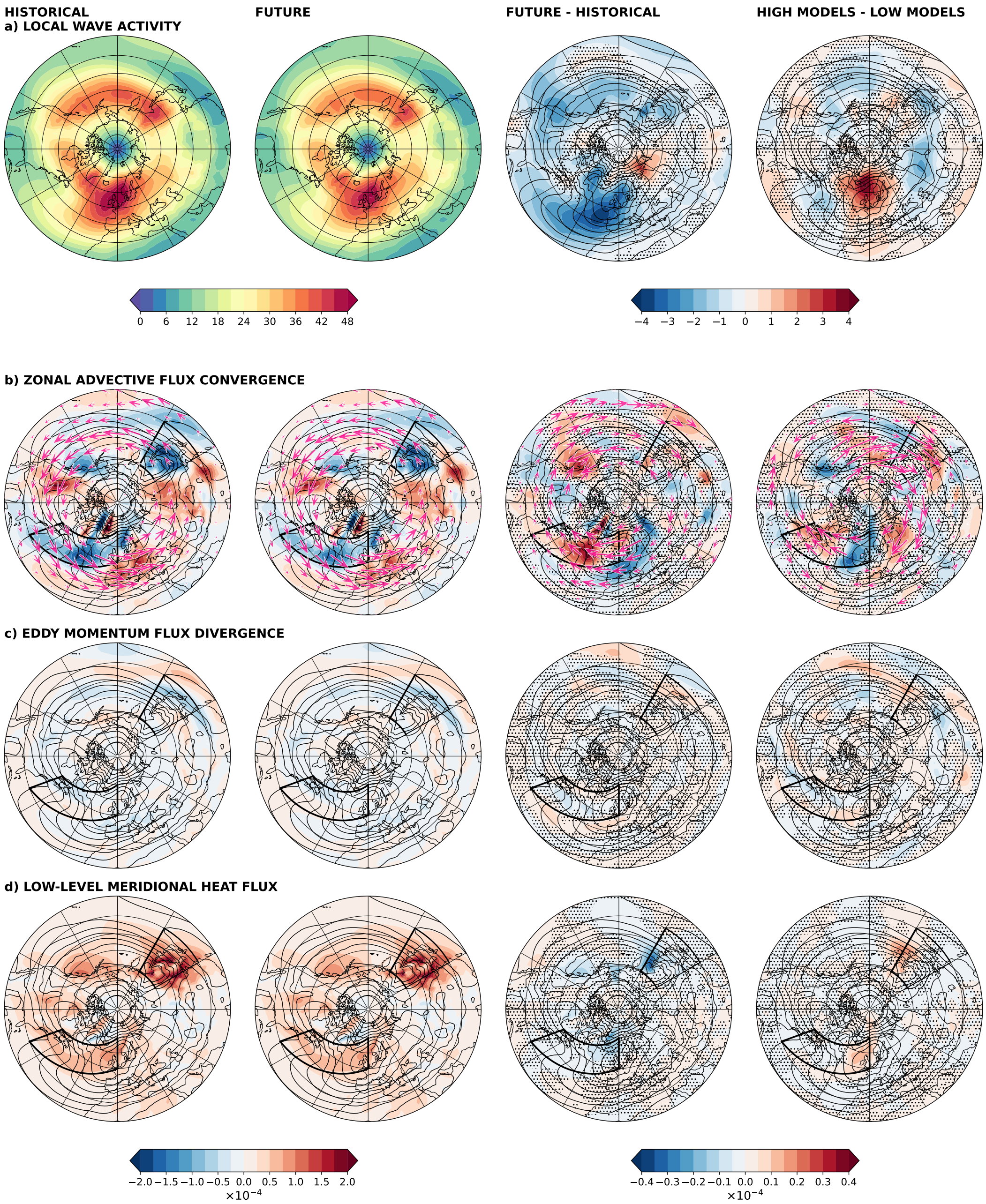

Figure 3. a) Same as Figure 1a, but for DJF climatology of historical (first column) and future (second column) simulations. b)-d) Same as Figure 2 but for DJF climatology of historical (first column) and future (second column) simulations. (Third column) difference between future and historical climatology and (fourth column) difference between future and historical climatology for high-resolution models minus that for low-resolution models of respective fields. Black contours indicate historical LWA DJF climatology of all models.

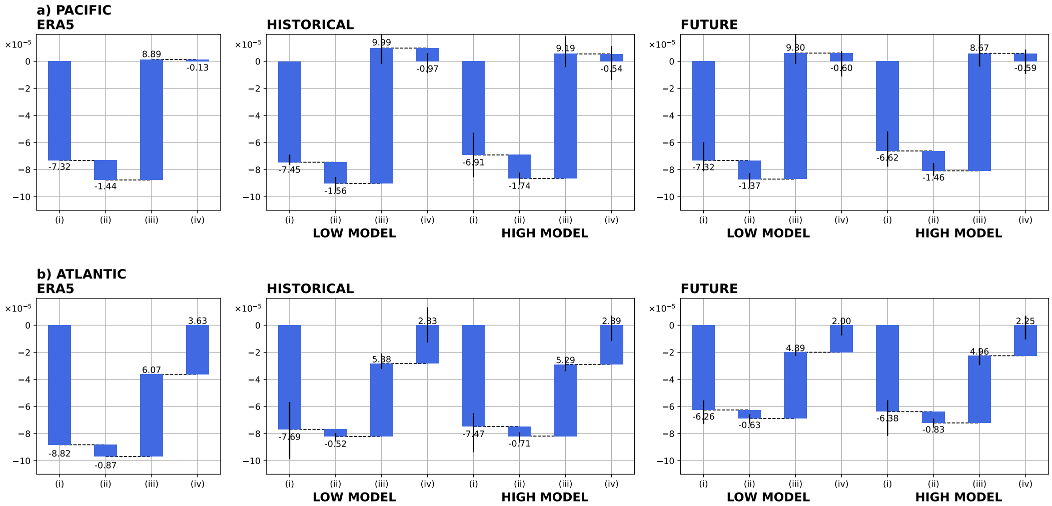

Figure 4. Waterfall chart of each term [m s^{-2}] comprised in the LWA time tendency equation (Equation 3) separately plotted for a) Pacific and b) Atlantic sectors (encircled areas in Figure 2 and 3), computed with ERA5 (first column), with historical runs, separately for low-resolution models and high-resolution models (middle column), and with future runs (last column). Black bars indicate the range of values across all the models used.

References

Athanasiadis, P. J., Ogawa, F., Omrani, N.-E., Keenlyside, N., Schiemann, R., Baker, A. J., ... Gualdi, S. (2022, 11). Mitigating climate biases in the mid-latitude north atlantic by increasing model resolution: Sst gradients and their relation to blocking and the jet. *Journal of Climate*, *35*, 6985-7006. Retrieved from `https://journals.ametsoc.org/view/journals/clim/35/21/JCLI-D-21-0515.1.xml` doi: 10.1175/JCLI-D-21-0515.1

Barnes, E. A. (2013). Revisiting the evidence linking arctic amplification to extreme weather in midlatitudes. *Geophysical Research Letters*, *40*, 4734-4739. doi: 10.1002/grl.50880

Boville, B. A. (1991, may). Sensitivity of Simulated Climate to Model Resolution. *J. Clim.*, *4*(5), 469–485. Retrieved from `http://journals.ametsoc.org/doi/10.1175/1520-0442(1991)004{\%}3C0469:SOSCTM{\%}3E2.0.CO;2` doi: 10.1175/1520-0442(1991)004⟨0469:SOSCTM⟩2.0.CO;2

Cattiaux, J., Peings, Y., Saint-Martin, D., Trou-Kechout, N., & Vavrus, S. J. (2016). Sinuosity of midlatitude atmospheric flow in a warming world. *Geophysical Research Letters*, *43*, 8259-8268. doi: 10.1002/2016GL070309

Chen, G., Lu, J., Burrows, D. A., & Leung, L. R. (2015). Local Finite-Amplitude Wave Activity as an Objective Diagnostic of Midlatitude Extreme Weather. *Geophys. Res. Lett.*, *42*. doi: 10.1002/2015GL066959

Coumou, D., Lehmann, J., & Beckmann, J. (2015). The weakening summer circulation in the Northern Hemisphere mid-latitudes. *Science (80-.).*(March), 1–8.

Davini, P., & D'Andrea, F. (2020). From cmip3 to cmip6: Northern hemisphere atmospheric blocking simulation in present and future climate. *Journal of Climate*, *33*, 10021-10038. doi: 10.1175/JCLI-D-19-0862.1

Di Capua, G., & Coumou, D. (2016). Changes in meandering of the Northern Hemisphere circulation. *Environ. Res. Lett.*, *11*(9), 094028. Retrieved from `http://stacks.iop.org/1748-9326/11/i=9/a=094028?key=crossref.98f5b5d191331b0954b4bec87f0ee100` doi: 10.1088/1748-9326/11/9/094028

Francis, J. A., & Vavrus, S. J. (2012). Evidence linking arctic amplification to extreme weather in mid-latitudes. *Geophysical Research Letters*, *39*, 1-6. doi: 10.1029/2012GL051000

Grams, C. M., & Archambault, H. M. (2016). The key role of diabatic outflow in amplifying the midlatitude flow: A representative case study of weather systems surrounding western north pacific extratropical transition. *Monthly Weather Review*, *144*, 3847-3869. doi: 10.1175/MWR-D-15-0419.1

Haarsma, R. J., Roberts, M. J., Vidale, P. L., Catherine, A., Bellucci, A., Bao, Q., ... Storch, J. S. V. (2016). High resolution model intercomparison project (highresmip v1.0) for cmip6. *Geoscientific Model Development*, *9*, 4185-4208. doi: 10.5194/gmd-9-4185-2016

Hersbach, H., Bell, B., Berrisford, P., Hirahara, S., Horányi, A., Muñoz-Sabater, J., ... Thépaut, J. N. (2020). The era5 global reanalysis. *Quarterly Journal of the Royal Meteorological Society*, *146*, 1999-2049. doi: 10.1002/qj.3803

Huang, C. S., & Nakamura, N. (2016). Local finite-amplitude wave activity as a diagnostic of anomalous weather events. *Journal of the Atmospheric Sciences*, *73*, 211-229. doi: 10.1175/JAS-D-15-0194.1

Huang, C. S., & Nakamura, N. (2017). Local wave activity budgets of the wintertime northern hemisphere: Implication for the pacific and atlantic storm tracks. *Geophysical Research Letters*, *44*, 5673-5682. doi: 10.1002/2017GL073760

Joos, H., Sprenger, M., Binder, H., Beyerle, U., & Wernli, H. (2023, 1). Warm conveyor belts in present-day and future climate simulations - part 1: Climatology and impacts. *Weather and Climate Dynamics*, *4*, 133-155. doi: 10.5194/wcd-4-133-2023

Madonna, E., Wernli, H., Joos, H., & Martius, O. (2014). Warm conveyor belts in the era-interim dataset (1979-2010). part i: Climatology and potential vorticity evolution. *Journal of Climate*, *27*, 3-26. doi: 10.1175/JCLI-D-12-00720.1

Martin, J. E. (2021). Recent Trends in the Waviness of the Northern Hemisphere Wintertime Polar and Subtropical Jets. *J. Geophys. Res. Atmos.*, *126*(9), 1–15. doi: 10.1029/2020JD033668

Martineau, P., Chen, G., & Burrows, D. A. (2017). Wave events: Climatology, trends, and relationship to northern hemisphere winter blocking and weather extremes. *Journal of Climate*, *30*, 5675-5697. doi: 10.1175/JCLI-D-16-0692.1

Nakamura, N., & Huang, C. S. (2018). Atmospheric blocking as a traffic jam in the jet stream. *Science*, *361*, 42-47. doi: 10.1126/science.aat0721

Nakamura, N., & Solomon, A. (2010, nov). Finite-Amplitude Wave Activity and Mean Flow Adjustments in the Atmospheric General Circulation. Part I: Quasigeostrophic Theory and Analysis. *J. Atmos. Sci.*, *68*(11), 2783–2799. doi: 10.1175/2011JAS3685.1

Neal, E., Huang, C. S. Y., & Nakamura, N. (2022, 4). The 2021 pacific northwest heat wave and associated blocking: Meteorology and the role of an upstream cyclone as a diabatic source of wave activity. *Geophysical Research Letters*, *49*. Retrieved from `https://onlinelibrary.wiley.com/doi/10.1029/2021GL097699` doi: 10.1029/2021GL097699

Pfahl, S., Schwierz, C., Grams, C. M., & Wernli, H. (2015). Importance of latent heat release in ascending air streams for atmospheric blocking. *Nature Geoscience*, *8*, 610-615. doi: 10.1038/NGEO2487

Röthlisberger, M., Pfahl, S., & Martius, O. (2016). Regional-scale jet waviness modulates the occurrence of midlatitude weather extremes. *Geophysical Research Letters*, *43*, 10,989-10,997. doi: 10.1002/2016GL070944

Screen, J. A., & Simmonds, I. (2013). Exploring links between Arctic amplification and mid-latitude weather. *Geophys. Res. Lett.*, *40*(5), 959–964. doi: 10.1002/grl.50174

Tsujino, H., Urakawa, L. S., Griffies, S. M., Danabasoglu, G., Adcroft, A. J., Amaral, A. E., ... Yu, Z. (2020, 8). Evaluation of global ocean-sea-ice model simulations based on the experimental protocols of the ocean model intercomparison project phase 2 (omip-2). *Geoscientific Model Development*, *13*, 3643-3708. doi: 10.5194/gmd-13-3643-2020

Woollings, T., Barriopedro, D., Methven, J., Son, S. W., Martius, O., Harvey, B., ... Seneviratne, S. (2018). Blocking and its response to climate change. *Current Climate Change Reports*, *4*, 287-300. doi: 10.1007/s40641-018-0108-z

Yamamoto, A., Nonaka, M., Martineau, P., Yamazaki, A., Kwon, Y.-O., Nakamura, H., & Taguchi, B. (2021, 8). Oceanic moisture sources contributing to wintertime euro-atlantic blocking. *Weather and Climate Dynamics*, *2*, 819-840. Retrieved from `https://wcd.copernicus.org/articles/2/819/2021/` doi: 10.5194/wcd-2-819-2021